LETTER

Atomic force microscopy imaging of the albite (010) surface

Barney Drake

Imaging Services, P.O. Box 9981, Truckee, California 95737, U.S.A.

Roland Hellmann[*]

Université Joseph Fourier, L.G.I.T.-I.R.I.G.M., B.P. 53X, 38041 Grenoble Cedex, France

Abstract

A sample of Amelia albite was cleaved in air and the (010) surface was subsequently imaged with an atomic force microscope. Detailed images, down to a scale of 30 × 30 Å, show that the surface is composed of six-sided, interconnected, en-echelon rings. Taking into account the number of O atoms (32 per unit cell) and their large ionic radii, we assume that the structures imaged represent O rings. Using Fourier transforms of the surface scans, we obtained two primary nearest neighbor distances: 4.7 and 4.9 ± 0.5 Å. By superimposing a (010) bulk structure projection onto an image, we were able to directly compare the surface structure with that of the bulk. The close superposition agreement between the ring structures in the AFM images and the projections indicates that the surface configuration of atoms is close to an ideal termination of the bulk structure.

Introduction

With the advent of scanning tunneling microscopy (STM) (Binnig et al., 1982) and atomic force microscopy (AFM) (Binnig et al., 1986), scientists in a variety of disciplines have been able to obtain unprecedented information on the atomic-scale structure and topography of surfaces. In the field of mineralogy, nearly all surface AFM-STM studies to date have imaged structurally simple minerals that cleave along well-defined atomic planes.

Two very recent studies have focused on framework silicate minerals, quartz and albite. Gratz et al. (1991) investigated the development of etch pits and the movement of atomic-scale ledges during the dissolution of quartz. Hochella et al. (1990) studied the surface of albite both with AFM and low-energy electron diffraction (LEED). Their AFM images reveal the presence of nanometer-sized surface pits and depressions. Both of these studies did not achieve atomic-scale resolution, however.

In this paper we use AFM images to determine the atomic-scale surface structure and topography of the (010) plane of albite. We have chosen albite for AFM imaging for two main reasons: its general geological importance in the Earth's crust and the fact that its bulk structure is well known. In addition, the chemical and structural evolution of the near-surface region after alteration has been studied with a variety of spectroscopic techniques, both for albite (Hellmann et al., 1990), and other feldspars (Casey et al., 1989). Thus, this present study should serve as a basis for providing new and complementary information on the surface structure and reactivity of albite surfaces.

The images reported here show with great detail the atomic structure and topography of a natural (010) cleavage surface. The goal of this study is to determine whether the surface is an ideal termination of the bulk structure. We base our results on a comparison of measured surface orientations and nearest neighbor distances from the AFM images with those from a surface projection of the bulk structure, as deduced from X-ray and neutron diffraction data in the literature. From this comparison, we note that there is no evidence for surface reconstruction, and in general terms, the correspondence between the surface and bulk structures is very close. The largest measured differences in nearest neighbor distances was 0.2–0.4 Å. The measured differences may be due to a variety of reasons, as we discuss later on.

Experimental

Atomic force microscope

The NanoScope II contact mode AFM from Digital Instruments used in this experiment is based on an optical lever design (Meyer and Amer, 1988; Alexander et al., 1989) that has been described in detail in previous publications (Ruger and Hansma, 1990). In this study imaging forces ranged from 10 to 100 nN using 120-μm Si_3N_4 cantilevers from Digital Instruments ($k \approx 0.6$ N/m) with integral tips. Lower forces can be used, but improved image quality is usually obtained on rigid crystalline materials at higher forces. The AFM can operate under a variety of fluids; however, the images presented here were all taken in air using a piezotranslator with a scan area 1 μm × 1 μm.

This study utilized low albite from Amelia Court House, Virginia; it was supplied by Wards Scientific Establish-

---

ment. The specimen used was compositionally pure, end-member albite, as was determined by three previous microprobe analyses of various surface (010) regions (Hellmann et al., 1990). The AFM images are based on a single cleavage fragment that was chosen for its mirrorlike flatness. No special sample treatment was carried out. Two sets of AFM images were taken, about 3 months apart, of the same specimen surface. The sample was left exposed to air between imaging sessions.

The first set of images was made with a single cantilever. Imaged areas were approximately 100 Å apart. The second set of images was taken with three separate cantilevers; therefore, the images we obtained are of different and totally random areas. Any particular area was investigated for up to half an hour. In all cases, there was no noticeable difference in the images as a function of time. Processed images were plane fitted and then filtered using a two-dimensional fast Fourier transform (2DFFT); all of the peaks were kept, but high frequency noise was selectively removed.

Albite mineral relations

The albite structure is characterized by triclinic symmetry, with 52 atoms per unit cell ($Na_4Al_4Si_{12}O_{32}$). The cell dimensions are $a = 8.142$ Å, $b = 12.785$ Å, $c = 7.159$ Å, $\alpha = 94.19°$, $\beta = 116.61°$, $\gamma = 87.68°$ (Harlow and Brown, 1980). The albite structure is typically characterized as having a double crankshaft chain. In a projection in the **ac** plane, the double crankshaft takes the form of interconnected chains of four-membered rings of Si and Al tetrahedra, where alternating rings are either high or low with respect to the **b** axis. The alternating sequence of high and low rings gives rise to the crankshaft structure. The chains of fourfold rings are interconnected by bridging O atoms. Na atoms occupy charge-balancing interstitial sites.

RESULTS AND INTERPRETATIONS

The extraordinary detail of the image in Figure 1 allows one to clearly distinguish individual, six-sided rings (this can be best appreciated by viewing the ring in the center of the image). The six apices of each ring are characterized by nodelike structures. The rings are all interconnected, such that each apparent edge is shared by two adjacent, en-echelon rings. Each six-sided ring is slightly elongated and tilted within the plane of the image, subparallel to the **y** axis in the image. The central cavity of each ring is also elongated in the same direction. Because of the irregular nature of the rings, our measurements of center-to-center cavity distances range from 4.0 to 5.0 Å.

The elongated nature of the central ring in Figure 1 results in two sets of internode distances. The shorter node distance (as measured between the cross hairs) is 1.8 Å; the corresponding node distance on the opposite side of the cavity is 2.0 Å. The other four longer node distances range from 3.0 to 3.6 ± 0.3 Å. Examination of the six nodes in the central ring reveals that their heights
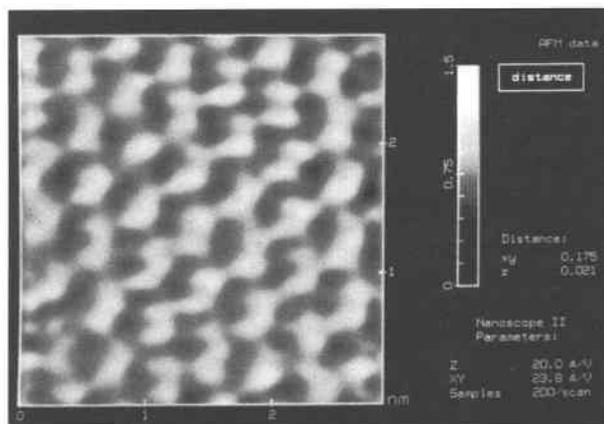

Fig. 1. A filtered (2DFFT) AFM image of a (010) surface 30 × 30 Å (different area from Fig. 1). Note the six-sided ring in the center of the image, with its six distinct apical nodes. The sinuous chain pattern composed of light and dark areas is caused by the faintness of one or two of the six sides of each ring.

vary less than 0.5 Å. The measured difference in heights of the two nodes marked by the cross hairs is only 0.21 Å.

The degree of connectedness between the nodes is quite variable, however. This point is well illustrated by examination again of the six nodes of the central ring. The faint nature of certain connections is indicative of atoms lying at elevations below the node atoms. It is important to note the periodicity and constant orientation of connections that are either high or low. The corrugated pattern formed by the alignment of the ring cavities is a direct result of certain internode atoms positioned low enough such that the connections are almost indiscernible.

In order to better understand the structure shown in the AFM images, we make a comparison with a crystallographic projection. The projection (EMS software) is based on atomic coordinates derived from an X-ray and neutron diffraction structure refinement of the albite structure (Harlow and Brown, 1980). In Figure 2 we show four unit cells projected onto the (010) plane. We have not adopted the standard ionic radii of Shannon and Prewitt (1969); instead, for the sake of clarity, we use the following radii: $Si^{4+} = 0.20$, $Al^{3+} = 0.20$, $O^{2-} = 0.50$, $Na^{1+} = 0.70$ (all in Å). It is easily seen that O atoms, being large and also the most numerous (32 per unit cell), determine the structural outline of the rings. Even though the Na atoms have large radii, there are only four of them per unit cell. The inconspicuous Si and Al atoms, occupying the center of each tetrahedral unit, possess radii that are much smaller than those of O and Na. The most conspicuous feature in Figure 2 is the presence of both parallel and offset interconnected rings of O atoms. The O atoms form elongated ring structures, with one complete ring per unit cell. The general outline of each ring is suggestive of a six-sided geometry.

In Figure 3 we superimpose a projection over the same filtered AFM image of the area 30 × 30 Å shown in
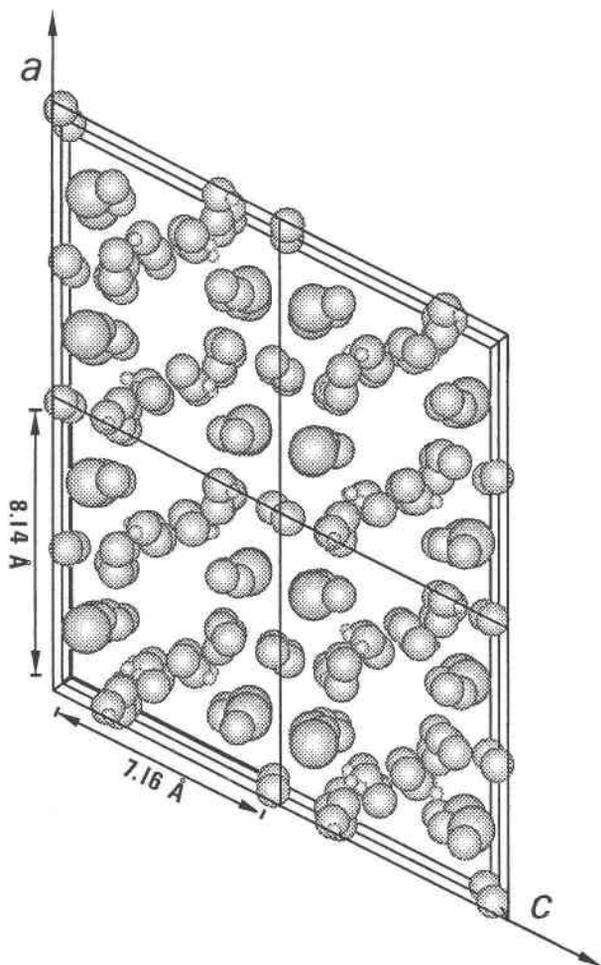
Fig. 2. A four unit-cell projection of the bulk feldspar structure onto the **ac** (010) plane. The projection is based on X-ray and neutron diffraction data (Harlow and Brown, 1980). For the sake of clarity, we use the following radii: Si^{4+} = 0.20, Al^{3+} = 0.20, O^{2-} = 0.50, Na^{1+} = 0.70 (all in Å). There is one complete, six-sided ring per unit cell. Note that O atoms predominate in the rings.
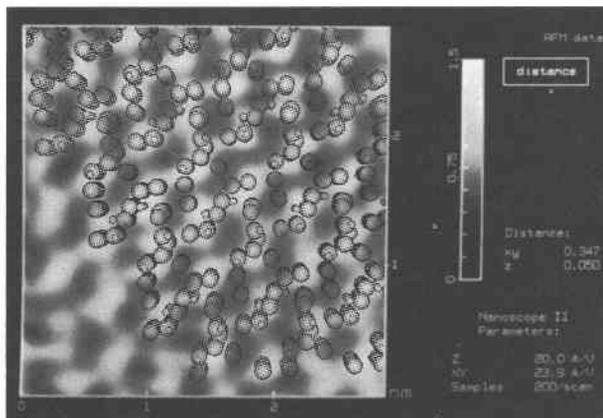

Fig. 3. Superposition of about 14 unit cells of the bulk (010) projection onto the same AFM image shown in Figure 1. Note that this projection represents a slice from 0 to 5 Å along the **b** axis. The **ac** axes are shown for reference. The scale of the image and the projection are the same. A slight mismatch in the O ring spacing is apparent—see text for details.

Figure 1. The projection is based not on the full unit cell, but rather only on a slice along the **b** axis ranging from 0 to 5.1 Å. We chose this slice since the cleavage plane most probably forms where the density of Si-O-Si bonds is lowest. Based on (001) and (100) projections, the Si-O-Si bond density is at a minimum at 0, 0.5, and 1.0 along **b**; this also corresponds to the Na atom positions along **b**. Therefore, we have assumed that the plane being imaged is representative of slightly less than half the unit cell in the **b** direction.

The orientation of the projection with respect to the AFM image is of course very important to the correct interpretation of the surface structure. The method we used for orienting the projection was based on comparing the Fourier transforms of the images with that of the projection. We obtained three separate, two-dimensional, fast-Fourier transforms of the spatial information gener-

ated by the tip scanning the surface. Two average nearest neighbor distances were dominant: 4.7 and 4.9 ± 0.5 Å. The two dominant nearest neighbor distances of the crystallographic projection were determined to be 4.4 and 4.7 ± 0.2 Å. The differences in interplanar orientations between the images and the projection were on the order of ±3°.

Using the measured interplanar distances and orientations of the projection, we constructed a set of geometric projections, the resulting diagram being mathematically analogous to a Fourier transform of the projection. We chose the best fitted solution (superposition) that was possible between the two sets of Fourier transforms—this was the basis for the orientation of the projection with respect to the AFM image.

The superposition of the projection of approximately 14 unit cells onto the image (Fig. 3, both at the same scale) shows that there is a good correlation between the ring structures and the ring cavities of the projection and the image. However, the inter-ring spacing in the **a** and **c** directions is not quite perfect. This is caused by a slightly different periodicity in the ring structures as well as a certain lack of one-to-one correspondence in atoms or atom clusters between the projection and the image.

At this point we note that the approach we have taken is simplistic for the very complex nature inherent in the determination of surface structure. There is probably no one unique solution to superimposing the projection on the images. This is in part a function of the accuracy of the interplanar distances and orientations obtained from the Fourier transforms of the images and the projections. The problem is compounded by the fact that the choice of projection slice, as well as thickness along **b**, influences the orientations and interplanar distances measured on the geometric constructions.

The causes for instrumental error are also quite varied.

A broad group of instrumental errors can be attributed to thermal drift, piezo creep, cantilever buckling, etc. These types of error make the calibration of the AFM instruments very important. The calibration of our AFM images is based on measured nearest neighbor distances for muscovite and graphite. For muscovite, our nearest neighbor values translate to a ring-to-ring spacing of 5.3 ± 0.5 Å, this being well in accord with the value of 5.20 Å accepted in the literature (Deer et al., 1978); for graphite our measured average ring-to-ring distance of 2.4 ± 0.3 Å compares well with the accepted value of 2.46 Å. These two calibration checks confirm that the instrument error, which influences the accuracy of the image scales, is approximately 5–10%.

Another possible reason for error in interplanar spacing and orientation is related to tip-sample interactions. Since the AFM image is a product of the tip-sample interaction, tip structure plays a very important role in image quality and accuracy (Gould et al., 1989). One problem may be due to the fact that when the tip scans over a structure that has a very high density of atoms lying at disparate heights, multiple surface-tip interactions may occur. Thus, the measured interplanar distances may not be amenable to straightforward interpretation. We must bear in mind that tip-sample interactions may play a more important role in the imaging of complex framework silicate structures than of sheet silicate structures.

At this point, the natural question arises as to whether we have achieved true atomic resolution. Certainly at the scale shown in Figures 1 and 3, individual O atoms, with an ionic radius estimate of 1.21 Å (Shannon and Prewitt, 1969), should be distinguishable. From the projection, it is evident that the O atoms of each unit cell are quite closely spaced. The probable overlap of atoms is why we would hesitate to assign identities to the various bulbous nodes of the six-sided rings in the image. At this point, we prefer to think of these nodes, as well as the connections between them, as representing atom clusters.

CONCLUSIONS

The atomic force microscope images we present in this paper reveal detail at the atomic level of the surface topography and configuration of atoms on the albite (010) surface. The superposition of the (010) projection on the AFM image (Fig. 3) shows the crystallographic orientation of the **a** and **c** axes, as well as the one-to-one correspondence between the rings in the projection and the six-sided ring structures in the images. As is apparent from the projection, the majority of ring atoms are O atoms. Because of the complex nature of the structure and the overlap (in the **z** direction) of atoms, we cannot actually identify the individual atoms at surface sites. At present only groups of atoms can be assigned to particular nodes of the individual rings.

The nearest neighbor distances measured on the images are greater by 0.2–0.4 Å than those measured on the crystallographic projection. This indicates that either the measured AFM distances are in error, or lateral surface relaxation may be responsible for the mismatch in distances. A recent AFM-LEED study (Hochella et al., 1990) provides evidence that the (010) albite surface does show a slight degree of lateral surface relaxation. Therefore, the surface may not represent a perfect termination of the bulk structure. Nonetheless, our results show that major differences do not exist between the observed surface structure and that which would be predicted based on knowledge of the bulk structure. A refinement of these results, based on further experimental work as well as electronic structure calculations, should certainly be a worthwhile direction for future research.

REFERENCES CITED

Alexander, S., Hellemans, L., Marti, O., Schneir, J., Elings, V., Hansma, P.K., Longmire, M., and Gurley, J. (1989) An atomic-resolution atomic-force microscope implemented using an optical lever. Journal of Applied Physics, 65, 164–167.

Binnig, G., Rohrer, H., Gerber, Ch., and Weibel, E. (1982) Surface studies by scanning tunneling microscopy. Physical Review Letters, 49, 57–61.

Binnig, G., Quate, C.F., and Gerber, Ch. (1986) Atomic force microscope. Physical Review Letters, 56, 930–933.

Casey, W.H., Westrich, H.R., Arnold, G.W., and Banfield, J.F. (1989) The surface chemistry of dissolving labradorite feldspar. Geochimica et Cosmochimica Acta, 53, 821–832.

Deer, W.A., Howie, R.A., and Zussman, J. (1978) An introduction to the rock-forming minerals, 528 p. Longman, London.

Gould, S.A.C., Burke, K., and Hansma, P.K. (1989) Simple theory for the atomic-force microscope with a comparison of theoretical and experimental images of graphite. Physical Review B, 40, 5363–5366.

Gratz, A.J., Manne, S., and Hansma, P.K. (1991) Atomic force microscopy of atomic-scale ledges and etch pits formed during dissolution of quartz. Science, 251, 1343–1346.

Harlow, G.E., and Brown, G.E., Jr. (1980) Low albite: An X-ray and neutron diffraction study. American Mineralogist, 65, 986–995.

Hellmann, R., Eggleston, C.M., Hochella, M.F., Jr., and Crerar, D.A. (1990) The formation of leached layers on albite surfaces during dissolution under hydrothermal conditions. Geochimica et Cosmochimica Acta, 54, 1267–1281.

Hochella, M.F., Jr., Eggleston, C.M., Elings, V.B., and Thompson, M.S. (1990) Atomic structure and morphology of the albite {010} surface: An atomic-force microscope and electron diffraction study. American Mineralogist, 75, 723–730.

Meyer, G., and Amer, N.M. (1988) Novel optical approach to atomic force microscopy. Applied Physics Letters, 53, 1045–1047.

Ruger, D., and Hansma, P.K. (1990) Atomic force microscopy. Physics Today, 43, 23–30.

Shannon, R.D., and Prewitt, C.T. (1969) Effective ionic radii in oxides and fluorides. Acta Crystallographica, B25, 925–946.